Aerosol-cloud drop concentration closure in warm cumulus

W.C. Conant[1], T.M. VanReken[1], T.A. Rissman[1], V. Varutbangkul[1], H.H. Jonsson[2], A. Nenes[3], J.L. Jimenez[4], A.E. Delia[4], R. Bahreini[1], G.C. Roberts[5], R.C. Flagan[1], and J.H. Seinfeld[1*]

[1]*Departments of Environmental Science and Engineering and Chemical Engineering, California Institute of Technology, Pasadena, California*

[2]*CIRPAS, Naval Postgraduate School, Monterey, California*

[3]*Schools of Earth and Atmospheric Sciences and Chemical and Biomolecular Engineering, Georgia Institute of Technology, Atlanta, Georgia*

[4]*Department of Chemistry & Biochemistry, CIRES, University of Colorado at Boulder, Colorado*

[5]*Center for Atmospheric Sciences, Scripps Institution of Oceanography, University of California, San Diego, California*

[*]To whom correspondence should be directed. E-mail: seinfeld@caltech.edu; phone: (626) 395-4635; fax: (626) 796-2591.

Abstract. Our understanding of the activation of aerosol particles into cloud drops during the formation of warm cumulus clouds presently has a limited observational foundation. Detailed observations of aerosol size and composition, cloud microphysics and dynamics, and atmospheric thermodynamic state were collected in a systematic study of 21 cumulus clouds by the CIRPAS Twin Otter aircraft during NASA's Cirrus Regional Study of Tropical Anvils and Cirrus Layers – Florida Area Cirrus Experiment (CRYSTAL-FACE). An "aerosol-cloud" closure study was carried out in which a detailed cloud activation parcel model, which predicts cloud drop concentration using observed aerosol concentration, size distribution, cloud updraft velocity, and thermodynamic state, is evaluated against observations. On average, measured droplet concentration in adiabatic cloud regions is within 15% of the predictions. This agreement

is corroborated by independent measurements of aerosol activation carried out by two cloud condensation nucleus (CCN) counters on the aircraft. Variations in aerosol concentration, which ranged from 300 cm^{-3} to 3300 cm^{-3} drives large microphysical differences (250 cm^{-3} – 2300 cm^{-3}) observed among continental and maritime clouds in the South Florida region. This is the first known study in which a cloud parcel model is evaluated in a closure study using a constraining set of data collected from a single platform. Likewise, this is the first known study in which relationships among aerosol size distribution, CCN spectrum, and cloud droplet concentration are all found to be consistent with theory within experimental uncertainties much less than 50%. Vertical profiles of cloud microphysical properties (effective radius, droplet concentration, dispersion) clearly demonstrate the boundary layer aerosol's effect on cloud microphysics throughout the lowest 1 km of cloud depth. On-board measurements of aerosol hygroscopic growth and the organic to sulfate mass ratio are related to CCN properties. These chemical data are used to quantify the range of uncertainty associated with the simplified treatment of aerosol composition assumed in the closure study.

1. Introduction

Satellite and aircraft observations have corroborated predictions that particulate pollution increases cloud albedo and decreases precipitation efficiency [*Twomey*, 1977; *Albrecht et al*., 1989; *Rosenfeld and Lensky*, 1998; *Ackerman et al*., 2000]. Because such effects alter Earth's climate by perturbing the radiation balance and hydrological cycle, they are called indirect effects of aerosol on climate, or simply "indirect effects" [*Houghton et al.*, 2001]. To have confidence in predictions of indirect effects, it is

necessary to develop physically-based and observationally-validated models of the sensitivity of cloud microphysics to the properties of the cloud condensation nuclei (CCN) on which the cloud forms. The most fundamental of these models is the adiabatic parcel model, which predicts cloud drop concentrations within ascending air parcels by simulating the transfer of water vapor and heat between the adiabatically cooling parcel and the CCN within using a first principles treatment of chemical and thermodynamic processes. These models are used as tools to formulate and validate the relatively simpler parameterizations that are used in cloud resolving models and global climate simulations [e.g. *Nenes and Seinfeld*, 2003].

In an attempt to give such models a firm observational foundation, two closure studies were conducted during CRYSTAL-FACE. The first of these studies [*VanReken et al*., 2003] find that measured CCN concentrations at 0.2% and 0.85% supersaturations agree within 10%-20% of that predicted by Köhler theory given measured aerosol concentration and size distribution. This is termed aerosol-CCN closure. If chemical and kinetic effects on cloud activation are relatively minor, one could proceed to predict cloud drop number concentration (CDNC) directly from the measured CCN spectrum and observed updraft velocity in a CCN-CDNC closure [e.g. *Snider and Brenguier*, 2000]. Studies that attempt CCN-CDNC closure have generally been successful within a factor of about 50% [*Twomey and Warner*, 1967; *Fitzgerald and Spyers-Duran*, 1973, *Snider and Brenguier*, 2000]. In contrast, aerosol-CCN closure attempts have met with more limited success, such that predicted CCN often exceeds measured values [see review by *Chuang et al*., 2000]. The lack of aerosol-CCN closure brings into question either 1) our fundamental understanding of the role of aerosol composition on the CCN spectrum

("chemical effects", see *Nenes et al.,* [2002]), or 2) the techniques used to determine CCN spectrum or composition and mixing state. If CCN instrument bias is the source of the problem, however, this has implications for previous studies that found CCN-CDNC closure. A different strategy is taken here, in which a cloud model that predicts cloud drop concentration directly from updraft velocity and the aerosol physicochemical properties is evaluated against observations. This is termed aerosol-CDNC closure, in which the computation of CCN spectrum as an intermediary step is implicit. Taken together, aerosol-CCN closure and aerosol-CDNC closure provide a rigorous test on our understanding of how aerosol controls cloud microphysics.

CRYSTAL-FACE was conducted during July, 2002 from Boca Chica Naval Air Station near Key West, Florida (Figure 1). The CIRPAS Twin Otter, one of six aircraft deployed during CRYSTAL-FACE, provided redundant and calibrated measurements of aerosol concentration and size distribution from 0.003 μm – 5 μm; mass concentrations of sulfate, organic carbon, nitrate, and ammonium from 0.1 μm – 0.6 μm; cloud condensation nucleus (CCN) concentration at 0.2% and 0.85% supersaturation; cloud drop concentration and size distribution from 1 μm – 1600 μm; and absolute wind speed with 0.35 m s^{-1} accuracy, which is derived from a gust probe on the nose of the aircraft and internal navigation and GPS positioning systems following *Lenschow et al*. [1986] (Table 1). Cumulus clouds were characterized by flying several successively higher constant altitude legs, starting with one or two legs below cloud base to obtain the aerosol properties and thermodynamic state of the air entrained through cloud base; the final legs often ended more than 2500 m above cloud base. Nine flights were dedicated to this strategy during which 20 clouds were profiled. These flights were conducted over land

and ocean with concentrations of CCN(0.85%) ranging from 300 cm^{-3} to 3300 cm^{-3} and cloud core drop concentrations ranging from 250 cm^{-3} to 2300 cm^{-3}. These data provide a wide range of conditions necessary to evaluate models of aerosol effects on warm cumulus microphysics.

2. Aerosol-CDNC closure

The *Nenes et al*. [2002] model simulates the activation of aerosol into cloud drops by numerically integrating the equations describing the rate of transfer of heat and water vapor between the gas and particulate phases for a parcel rising at constant updraft velocity [e.g. *Pruppacher and Klett*, 1997]. Initial temperature, pressure, humidity, and updraft velocity are specified along with a sufficient number of lognormal modes required to describe the dry aerosol size distribution (4 modes are used here, divided into 50 size bins per mode). Dry aerosol composition (NH_4^+, SO_4^{2-}, Na^+ Cl^-) and insoluble aerosol fraction are specified separately for each mode. It is known that soluble gases (e.g. HNO_3) and various organic species may have chemical effects (i.e. partial solubility, surface activity, film-forming tendency) that influence the CCN spectrum and the cloud activation process [*Nenes et al*., 2002]. Although the model is designed to simulate such chemical effects, they are assumed negligible here. This model compares well with other explicit cloud activation models when standard cases are used as input [*Kreidenweis et al*., 2002]. Condensation coefficient for this study is taken to be 0.06 based on the laboratory studies of *Shaw and Lamb* [1999]. (Other laboratory studies have found values ranging from 0.03-0.3; the standard value assumed in most cloud models is 0.042 [*Pruppacher and Klett*, 1997].) Particle surface tension is taken to be that of liquid water.

Simulations are made for each cloud profiled during CRYSTAL FACE using aerosol properties and thermodynamic state measured beneath the cloud.

Aerosol observations used as input to the model are obtained separately for each cloud in the following manner. Dry aerosol size measured by the DACADS (10 nm – 800 nm) and the PCASP optical probe (100 nm – 2500 nm) in the sub-cloud legs are merged into a single size distribution, averaged, and parameterized in the form of four log-normal modes. Submicrometer modes are taken to be ammonium bisulfate, which is consistent with the observed AMS NH_4^+:SO_4^{2-} ratios. Supermicrometer modes are presumed to be NaCl. Over land, the AMS composition (100 nm – 600 nm) often showed significant organic carbon (OC) content. OC is generally less soluble than sulfate aerosol [e.g. *Prenni et al.*, 2003, *Gysel et al.,* 2004], and may reduce aerosol surface tension [*Facchini et al*., 1999]. These have opposite effects on the CCN spectrum, relative to sulfate aerosol. The impact of the reduced solubility on the CCN spectrum is smaller when the OC is internally mixed with sulfate. Because no comprehensive model for OC activation behavior yet exists, previous attempts at CCN prediction have typically implemented one of two assumptions: either OC is entirely insoluble and internally mixed with sulfate [e.g. *Snider and Brenguier*, 2000], or that OC is treated as equivalent to ammonium sulfate (which rapidly approaches the insoluble and internally mixed assumption in the limit of low OC fraction) [e.g. *Rivera-Carpio et al.*, 1996]. *VanReken et al.* [2003] show that the aerosol-CCN closure at 0.2% and 0.85% in CRYSTAL-FACE was accurate to within 10%-20% given an ammonium sulfate assumption, in spite of wide variability in observed AMS OC:SO_4^{2-} ratio. Given this good agreement we initially implement the simpler assumption that OC behaves like

sulfate aerosol for the purposes of cloud activation. The appropriateness of this assumption will be examined in detail in Section 4. In Section 5, we study the implications of varying composition through a series of sensitivity studies. Concentration measured by the DACADS is tested against that measured by a TSI 3010 CPC, which measures all aerosol particles greater than 12 nm. In clear-air cases with stable CPC concentrations (standard deviation over 100 s < 15% of the mean), the DACADS and CPC concentrations agree with a negligible mean bias and a root-mean-square deviation of 20%. The DACADS-CPC difference is not sensitive to total concentration or mean aerosol size, indicating no significant saturation or size dependent biases exist for the range of conditions observed here. The inlet system for the Twin Otter cabin instruments was tested in a wind tunnel experiment, in which the transmission of particles from 10 nm – 2500 nm was indistinguishable from unity.

The measured CCN spectrum is not taken as an input to the parcel model (see methods employed by *Twomey et al.* [1959], *Snider and Brenguier* [2000], and *Snider et al*, [2003] for examples). Instead, full Köhler theory is employed at each stage of droplet growth, using the measured aerosol properties described above. *VanReken et al*. [2003] show 10%-20% agreement between calculated and measured CCN concentrations at 0.2% and 0.85% during CRYSTAL-FACE assuming the aerosol composition is ammonium sulfate, which is similar to the assumption used here of ammonium bisulfate and sodium chloride. Thus the CCN spectrum implicitly assumed here when solving the droplet growth equations is consistent with the CCN observations. Certain chemical effects on droplet activation, such as those of surface-forming organic films [*Feingold and Chuang*, 2002] and water soluble gases [*Laaksonen et al.*, 1998] are not strictly

tested in aerosol-CCN closure. These effects can contribute to a lack of aerosol-CDNC closure, even in the event that there is good aerosol-CCN closure.

Observations of updraft velocity were taken from below cloud and cloud-base legs. For the remainder of this paper, "cloud base" refers to the lowest 100 m of these cumulus, which extended several kilometers in height and contained coherent updrafts hundreds of meters in horizontal extent. Updraft velocity is obtained from a combination of instruments, including a 5-hole gust probe on the nose of the aircraft, a pitot-static pressure tube, a CMIGITS GPS/INS system, and the Novatel GPS system. Calibrations for all wind variables are derived using the procedures outlined in *Lenschow* [1986]. The aircraft velocity estimated by the CMIGITS system was reprocessed using position data from the more accurate Novatel GPS, while retaining the short-period response characteristics of the CMIGITS INS, which is based on quartz accellerometers. Uncertainties in total airspeed, INS retrieved heading and pitch angles, GPS-retrieved aircraft velocity, and the accuracy of the gust probe differential pressure measurements combine for a total uncertainty in updraft velocity of 0.35 m s^{-1}. A number of model calculations are made for each cloud to obtain predicted CDNC(w) as a function of updraft velocity, w. Then, a representative average CDNC(predicted) is obtained from CDNC(predicted) = $\int CDNC(w)wn(w)dw / \int wn(w)dw$, where $n(w)$ is the observed distribution of updraft velocity below and within cloud base, and the w weighting is introduced to account for the higher mass flux across cloud base associated with stronger updrafts. This procedure produces CDNC predictions on average 0.5% less than simply using mass-flux weighted mean w.

Droplet concentrations were observed at 1-Hz (~50 m) resolution using the CAS (Cloud and Aerosol Spectrometer) optical probe on board the CAPS (Cloud, Aerosol, and Precipitation Spectrometer) integrated spectrometer system [*Baumgardner et al*., 2001]. The CAS measures droplet size from 0.5 μm – 60 μm in 20 size bins using a forward scattering principle similar to that of the FSSP-100 (Forward Scattering Spectrometer Probe). Relative to the FSSP-100, the CAS contains certain design improvements that have: 1) obviated the need for dead-time corrections at concentrations less than 26,000 cm^{-3} (at the Twin Otter airspeed of 50 m s^{-1}) due to improved electronics; 2) reduced the frequency of coincidence errors by reducing the viewing volume and refining detection techniques; and 3) allowed for spectra to be obtained at lower sizes and finer size resolution by increasing laser power. These improvements make the CAS ideal for studying cloud activation, which requires observations to be close to cloud base where droplets are still small and have activated sufficiently recently to dramatically improve the probability of finding nearly adiabatic conditions. Coincidence errors, which are typical of single-particle optical probes (e.g. *Baumgardner et al*. [1985] and *Burnet and Brenguier* [2002]), are estimated to decrease cloud drop concentrations by 1% at 800 cm^{-3}, and 10% at 7000 cm^{-3}. Corrections to CDNC are applied using the principles outlined in *Burnet and Brenguier* [2002] and the CAS instrument characteristics (viewing area = 0.112 mm^2; beam width = 0.1 mm). Due to an improved CAS detection algorithm, particles outside the depth-of-field (DOF) do not contribute to coincidence errors in concentration as much as in the FSSP probes (Baumgardner, personal communication, 2004). The CAS size measurement was calibrated before, during, and after the campaign using monodisperse polystyrene and glass beads. Viewing volume is

estimated to be accurate within 15% using geometric characterization of the CAS viewing area and typical uncertainties in flow rates (e.g. *Dye and Baumgardner* [1984]). The particular CAS flown on the Twin Otter has shown stable properties in calibration and performance over its lifetime. Observed liquid water content (LWC) is measured by integrating the CAS size distribution. The large cumulus cloud (H4.3) sampled on 6/27 provides an opportunity to test the LWC measured by the CAS probe. The core of this cloud exhibited an adiabatic profile in equivalent potential temperature (θ_e) and LWC for each pass from 500 m (base) to 1700 m, meaning that, at the core of the cloud, θ_e was constant to within 10% of the sub-cloud minus out of cloud θ_e difference, and LWC was within 10% of the adiabatic calculation. Coincidence-related sizing errors [*Burnet and Brenguier*, 2002] are estimated to cause a range of uncertainty in LWC from -.5% to +1% for this cloud, whose core contained droplet concentrations of 410 cm^{-3}. Coincidence uncertainties in LWC assume coincidence events can be caused by particles within the viewing volume outside the DOF, which is assumed to have an effective sampling volume equal to that within the DOF [*Dye and Baumgardner*, 1984; Baumgardner, personal communication, 2004]. (Although the viewing volume outside the DOF is 2-3 times that within the DOF, the signals from particles outside the DOF are significantly reduced, thus limiting their contribution to coincidence artifacts on droplet size.) Uncertainties in determining the adiabatic LWC profile are small when compared with literature uncertainty estimates (e.g. *Lawson and Blyth* [1998]), because cloud base itself was determined within 30 m through cloud base penetrations. This determination was made microphysically, by observing GPS altitudes at the point where a cloud drop mode emerged from the haze in the observed CAS size distribution (0.5 – 50 μm diameter).

Based on this accuracy in cloud base altitude the uncertainty in adiabatic LWC is better than 10% when more than 300 m above cloud base. Because this cloud consistently exhibited core LWC values within 10% of adiabatic calculations on each pass up to 1200 m above cloud base, a 15% uncertainty in CAPS LWC is taken. This can be used to evaluate uncertainties in mean droplet volume (nominal uncertainty 33%) and number concentration (nominal uncertainty 15%), the product of which is LWC. Assuming uncertainty estimates above are uncorrelated and normally distributed, the 15% accuracy in LWC confirms the uncertainty estimate in number concentration of 15%, and increases confidence in the sizing uncertainty estimate to within 18% for mean droplet volume, and 6% for volumetric average diameter.

Data for the model-observation comparison in cloud drop concentration are carefully screened to avoid the influences of entrainment mixing, which is not treated in the model simulations. First, droplets below 1 μm diameter are neglected as unactivated haze. (Alternative methods to define haze based on the minimum between the haze mode and the droplet mode produced equivalent results in determining droplet concentration.) Cloud drop concentration observations are selected based on the following criteria: 1) the cloud drop effective diameter is greater than 2.4 μm [$d_e = \langle d^3 \rangle / \langle d^2 \rangle$, where $\langle\rangle$ indicates an average over the size distribution > 1 μm]; 2) it is narrow, having geometric standard deviation, $\sigma < 1.5$; 3) it contains no droplets larger than 30 μm diameter (to eliminate precipitation); and 4) cloud edge observations are neglected (i.e. both the preceding and subsequent observations must satisfy criteria (1-3)). Furthermore, only the lowest passes through the cloud are taken, which were most often within 50 m of cloud base. Two methods are used to determine mean "cloud base droplet concentration" from

the remaining data. For Method 1, droplet concentration is averaged over those observations having LWC exceeding the mean adiabatic value. A range of adiabatic LWC values is determined separately for each cloud based on variability in lifting condensation level computed from sub-cloud measurements of pressure, water vapor mixing ratio, q_g, and potential temperature, θ, and by assuming a moist adiabatic ascent through the cloud. Bias errors in lifting condensation level due to biases in the thermodynamic measurements are reduced through the microphysical determination of cloud base altitude discussed above. The average is obtained by weighting with updraft velocity (positive values only) to represent the mass-flux through cloud base. The screening criterion that LWC exceeds the mean adiabatic value minimizes the potential for including cloud regions strongly affected by entrainment, which tends to reduce droplet concentration and LWC. Method 2 screening is based on the observation that CDNC often contributes a much larger source of variability than volumetric mean diameter, $<d^3>$ to LWC (in these regions near cloud base). This is characteristic of artifacts related to averaging over cloud boundaries or including sub-adiabatic parcels that have been subjected to inhomogeneous mixing processes. Thus Method 2 screening omits low LWC observations so that variance in ln(CDNC) < the variance in ln($<d^3>$). In this manner, those observations having the maximum LWC at each pass are selected, irrespective of the adiabatic prediction.

Most often, droplet concentrations derived using Method 2 are larger than those using Method 1. Two explanations are suggested below. Typically there is a range of humidity beneath each cloud that produces variability in the adiabatic LWC profile. The source for this range is that air entering cloud base is not undiluted boundary layer air,

but rather is a varying mixture of boundary layer air and lower tropospheric air that is typically drier and warmer, which often has different aerosol properties. If the sub-cloud measurements are somehow biased towards drier air due to limited sampling statistics, then the computed adiabatic LWC will be biased low. Because inhomogeneous mixing processes dominate over homogeneous mixing processes in these cloud regions, this bias would produce lower measured droplet concentrations. On the other hand, the range in LWC within the screened data may be a direct consequence of the variability in sub-cloud humidity. Higher humidity parcels may be associated with stronger updrafts that originated closer to the surface, which is a source of moisture, buoyancy, and CCN. This may explain the strong positive correlation between updraft velocity and CDNC which was often observed near cloud bases. Because it is not clear from the present measurements whether Method 1 or Method 2 more accurately isolates adiabatic parcels, each method will be used and differences will be interpreted as due to experimental uncertainty.

The aerosol-CDNC closure for 20 of the clouds using Method 1 screening is shown in Figure 2. A linear fit to the data (dashed line) has a slope of 1.03. The slope is statistically indistinguishable from unity, and the mean percent deviation is -12% with a standard deviation about the mean of 13%. The mean underprediction is comparable to the uncertainty in the measured number concentration. The standard deviation is comparable to the variability in the DACADS concentration used as input to the model. There is no statistically significant correlation between the modeled-observed CDNC difference and the following quantities: OC:SO_4^{2-} mass concentration ratio, modeled-measured CCN concentration, updraft velocity, updraft velocity variance, or total droplet

concentration. While these factors may influence the model-observation difference (as discussed in Sections 4 and 5), their combined effect does not exceed the experimental noise. Also shown in Figure 2 is the linear fit of the model predictions to Method 2 data. This can be considered a range of uncertainty related to the method used to differentiate adiabatic parcels from sub-adiabatic parcels. The slope using Method 2 is still indistinguishable from unity at 0.98. The mean deviation is larger at -16%, with a standard deviation about the mean of 15%.

The difference between Methods 1 and 2 of 4% combined with the 15% uncertainty in the CAS concentration measurement yield an estimated 16% uncertainty in the measured cloud base concentration. Uncertainty in modeled cloud drop concentration is 10% from a contribution of uncorrelated uncertainties: 5% from aerosol concentration, 0.5% from DACADS sizing uncertainty, 8% from updraft velocity uncertainty, and 5% from parcel modeling simplifications. Uncertainty in modeled values of CDNC are thus 11%. This yields a net experimental uncertainty of 20% in the model-observation comparison. The mean model-observation bias taking an average of Methods 1 and 2 for observed concentration is -14%. This bias is within with the estimated experimental uncertainty. We note that the model assumes that aerosol composition is pure ammonium bisulfate, which is not entirely consistent with the observed composition and hygrosocopic data presented in Section 4. The effect of varying the ammonium bisulfate assumption on the model-observation closure is discussed in Section 5.

3. Effects of aerosol on the vertical profile of cloud microphysics

A more comprehensive description of cloud microphysics must include the effects of entrainment mixing, as adiabatic parcel model predictions are only useful in regions where there is little or no mixing among parcels of differing histories. Outside of these "adiabatic cores", entrainment mixing alters droplet concentrations, size distribution, LWC, and cloud thermodynamics via complex and unresolved mechanisms. Cloud albedo and precipitation efficiency are very sensitive to both cloud drop concentration and the shape of the size distribution; thus, it will be useful to investigate the apparent relationships between aerosol, cloud drop concentration, and size distribution in sub-adiabatic cloud regions.

At the core of these uncertainties is the observation that the dispersion in the cloud drop size distribution generally exceeds that of model predictions. Likewise, dispersion tends to be greater in polluted clouds than in unpolluted clouds [*McFarquhar and Heymsfield*, 2001]. It is not clear whether this increase is due to activation of entrained aerosol [*Bower and Choularton*, 1988], the activation of interstitial aerosol within vertically accelerating parcels [*Segal et al.,* 2003], differential droplet growth rates due to chemical differences among droplets [*Liu and Daum*, 2002; *Feingold and Chuang,* 2002], or multiphase flow processes such as enhanced coalescence or supersaturation due to vortex spinout [*Shaw*, 2003].

To illustrate the large effect of aerosol on the vertical profile of cloud properties, two extreme examples from 6/27 (H4.3) and 7/18 (C10.1) are shown in Figure 3 with their respective adiabatic calculations. For each cloud, both peak effective radius and peak droplet concentrations maintained nearly adiabatic values through the lowest ~1 km of the cloud core. H4.3 exhibited an adiabatic core 1200 m above cloud base, whereas

C10.1 appeared to be more strongly influenced by entrainment, with adiabatic LWC values only in the lowest pass.

A variety of phenomena, including bimodal spectra, activation of entrained CCN, and evidence for a mixture of both homogeneous and inhomogeneous mixing processes, was observed from profiles taken in this study. For example, the points identified in Figure 3 as "activation of entrained air" in cloud H4.3 were characterized by high droplet concentrations, narrow size spectra, small effective radii, and were found within a strong updraft 900 m above cloud base. These features are identical to those of recently activated parcels found near cloud base, and are inconsistent with microphysical properties found in detraining, evaporating cloud parcels, which characteristically have broad dispersions and low concentrations. Likewise, the sub-adiabatic profile of LWC in C10.1 was accompanied by a positive gradient in droplet dispersion strong enough to maintain nearly adiabatic profiles of effective radius and droplet concentration. An in-depth evaluation of these phenomena is beyond the scope of this work, yet deserves further study given the array of instrumentation directed towards aerosol and cloud microphysical characterization.

4. Relationships among hygroscopic growth, CCN, and organic carbon

In Section 2, the model assumed CCN are composed of simple salts. In this section, we examine this assumption using observations of organic carbon and sulfate mass concentrations, hygroscopic growth, and CCN properties. These observations were made on the Twin Otter aircraft with relatively rapid time resolution (5 minutes for

composition) and thus can be used to capture variability in aerosol properties during a single flight.

It is widely acknowledged that the hygroscopic properties of organic carbon (OC) aerosol vary among differing species, and that OC aerosols generally behave differently than inorganic salts. Two important quantities relevant to OC hygroscopic properties are explored here: first is hygroscopic growth (defined below); second is critical supersaturation / CCN concentration. Compared with sulfate aerosol of the same dry diameter, OC aerosol generally produces fewer dissolved species per unit volume. This effect leads to smaller hygroscopic growth and higher critical supersaturation. Certain species of OC can even be insoluble and hydrophobic. In contrast, surface active OC species (esp. humics) have been found to reduce surface tension, hence decreasing the critical supersaturation of the aerosol relative to the case in which surface tension is not reduced [*Facchini et al*., 1999]. The effect of surface tension reduction is less apparent on hygroscopic growth, being noticeable only at small (< 100 nm) sizes. When OC is found in the same aerosol population as inorganic salts, such as sulfate, the degree to which these species are internally mixed within individual particles plays an important role in the aggregate hygroscopic properties of the aerosol population.

In light of these complicated and competing effects and the currently poor ability to speciate atmospheric organics, there is a need for observations to constrain the hygroscopic properties of OC-containing aerosol populations in various regions. Some insight into this behavior for the organic species observed during CRYSTAL-FACE is obtained and presented here using three measurements – the DACADS, which measures aerosol size distribution at dry (15%-20% RH) and moist (50% - 75%) relative

humidities; the Caltech CCN counter, measuring concentration of aerosol having critical supersaturations below 0.85%, and the AMS measurement of OC and SO_4^{2-} mass concentrations.

The hygroscopic growth factor of a particle, f(RH), is defined as the ratio of its equilibrium diameter, D(RH), at a specified relative humidity, RH, to its dry diameter, d: $f(\mathrm{RH}) = D(\mathrm{RH})/d$. In an arbitrary aerosol population, particles of a fixed dry size will have varying composition, and hence varying values of f(RH). The ideal instrument to measure f(RH) as a function of d is the tandem DMA, in which the distribution of f(RH) values is obtained for each dry size d (e.g. *Brechtel and Kreidenweis* [2000]). Given current instrument configurations, this measurement takes a prohibitively long time for aircraft sampling, during which aerosol properties would be varying considerably. In contrast to the tandem DMA, the DACADS used on the Twin Otter obtains size distributions from two identical DMA columns operating at different relative humidities. This method provides more limited information, in that the effect of chemical heterogeneities at each size is not obtained, but has the distinct advantage that complete size distributions are obtained every 100 s. An effective value of f(RH) is obtained from the DACADS data as a function of d using two methods (Figures 4A,B). The first method simply calculates the required (non-uniform) shift in diameter of the dry size distribution to reproduce the moist size distribution (Figure 4B). This method is subject to uncertainties related to differences in the size-dependent loss rates and calibration uncertainties between the dry and humid differential mobility analyzer (DMA) columns. The second method takes advantage of the fact that most size distributions exhibit distinct Aitken and accumulation size modes, each of which shifts coherently with relative

humidity (Figure 4A). In the second procedure, both the dry and humid size distributions are represented as two or three lognormal modes using a least-squares fitting technique. An effective f(RH) is determined for Aitken and accumulation modes separately based on the shift in mode diameter. Changes in the width of the mode may be due to chemical heterogeneity within the population. This method provides less information than Method 1, but does not suffer from size-dependent calibration and loss uncertainties as long as such uncertainties are slowly varying with size. To reduce sampling noise, each of the 11 days used in this study is sub-divided into two to six periods representing distinct atmospheric conditions (altitude range, over land vs. sea, presence or lack of significant concentrations of < 30 nm particles). All DACADS size distributions made within each period are averaged together before being analyzed for hygroscopic growth. To minimize the occurrence of cases in which the humid column is not sufficiently moist to deliquesce particles that were dry in the atmosphere, only observations with ambient RH > 60% are considered.

To relate observed hygroscopic growth factors to observed CCN concentrations, an effective cutoff diameter D_C(0.85%) is obtained from the CCN(0.85%) concentration and the dry DACADS size distribution. D_C(0.85%) is defined such that CCN(0.85%) = $\int_{D_C(0.85\%)}^{800nm} N(d)\mathrm{d}d$, where $N(d)$ is the DACADS-measured dry size distribution. For an aerosol population composed completely of ammonium sulfate, D_C (0.85%) would be approximately 32 nm. Less hygroscopic species would exhibit larger values of D_C(0.85%). For the observations presented here, D_C (0.85%) ranges from 20 nm – 60 nm, which generally falls within the Aitken mode. Thus the hygroscopic properties found at Aitken mode size ranges will be most relevant to the CCN(0.85%) closure. Figure 5A

illustrates the relationship between f(RH) of the Aitken mode to D_C(0.85%). Only cases in which Method 1 and Method 2 agree within 10% are included in the analysis. Variability in humid RH (which ranged from 50% to 75%) is a source of uncertainty in the following analyses (Figure 5B). The weak correlation between RH and f(RH) among the data used in this study indicates a small effect of RH variability relative to that of aerosol composition. The relationship between Aitken mode hygroscopic growth and D_C(0.85%) suggests that compositional variations are influencing both hygroscopic growth and critical supersaturation in a consistent manner. Data from marine flight C6 (7/10) are shown separately in Figures 5A,B, since the simultaneously low D_C(0.85%) and f(RH) values are unique. Sea salt has a very low activation diameter (D_C(0.85%) = 25 nm), and may not have been deliquesced in the humid DMA, which was operating near the NaCl crystallization point of 62% RH. It is conceivable tha small sea-salt particles contributed significantly to the Aitken mode concentrations on this flight (the open sea wind speed at 50 m altitude ranged from 7-12 m s^{-1}), although fine sea-salt concentrations in excess of 100 cm^{-3} exceed even the surf-zone observations of *Clarke et al*. [2003].

Overlain on Figure 5A is the relationship between D_C(0.85%) and f(RH) obtained from model calculations assuming an internal mixture of ammonium sulfate solution and insoluble material. The curve corresponds to RH=63%, the horizontal bars represent the effect of varying RH from 59% to 69% in the f(RH) calculation. Two model curves are shown for Fig. 5B to illustrate the expected f(RH) for pure ammonium sulfate aerosol, and that for a 50/50 volumetric mix of sulfate and insoluble material (e.g. 35% OC by mass).

While D_C(0.85%) is more uniquely related to composition than CCN concentration, it is relevant to examine the relationships between hygroscopic growth and CCN concentration to bound the effect variations in hygroscopic growth have on CCN(0.85%). Figure 6 illustrates the percent difference between observed CCN(0.85%) to that predicted assuming the DACADS dry size distribution assuming ammonium sulfate (i.e. D_C(0.85%) = 32 nm), plotted vs. f(RH). The variability in CCN concentration falls within the range of -30% to +20%, with one outlier approaching -60% (from C20), and this variability is clearly associated with the hygroscopic growth factor for the Aitken mode.

Last, we explore the relationship between OC and hygroscopic behavior. D_C(0.85%) is plotted vs. the ratio of OC:SO_4^{2-} mass concentrations observed by the AMS for 100 nm – 600 nm diameter particles in Figure 7. Two regimes exist. In the first regime, where OC:SO_4^{2-} mass ratio is < 0.5, a very weak relationship exists between CCN cutoff diameter and OC fraction, despite a large variability in D_C(0.85%). In the second regime, for which OC:SO_4^{2-} > 0.5, cutoff diameter increases with increasing OC fraction, indicative of the expected lower hygroscopicity of OC species. The majority of these high OC:SO_4^{2-} observations were made on flights C10 and C11 (7/18/02). Backward Lagrangian trajectories computed from the NOAA HYSPLIT [*Draxler*, 1992] model for this day estimate that the airmass below 2000 m resided over the Florida peninsula for over 48 hours in a slow, southerly flow. This contrasts with the other days studied here, in which the airmasses resided over land for less than 24 hours. An interesting relationship between OC and f(RH) appears for the cases when OC:SO_4^{2-} < 0.5 (Figure 8A). There is a general decrease in the hygroscopic behavior of the Aitken

mode when OC fractions increase from 0.1 to 0.5. An interpretation of this result must take into account that the bulk of AMS mass is taken from sizes larger than those in the Aitken mode, and that the accumulation mode shows a much weaker relationship between hygroscopic growth and OC:SO_4^{2-} ratio relative to the Aitken mode (Figure 8B). These results imply that OC plays a strong role in Aitken mode hygroscopicity, and a weaker role in accumulation mode hygroscopicity. These observations are consistent with accumulation mode particles being internal mixtures of OC and SO_4^{2-}.

Despite the relationships seen among f(RH), D_C(0.85%) and OC:SO_4 mass ratios, there is no statistically significant correspondence between each of these three observations and the degree of aerosol-CDNC closure. The first three quantities are measured in longer (6-60 minutes) out-of-cloud periods, which allows for much reduced sampling uncertainty, whereas CDNC and updraft velocity are taken from relatively shorter (tens of seconds) sampling periods within cloud base regions. Despite this increase in sampling uncertainty, it is notable that the standard deviation between the observations and the models of CDNC is of order 15%. This suggests that the range of variation in CCN concentration that is related to aerosol hygroscopicity (Figure 6) is an upper limit on the influence composition has on CDNC in this study.

5. Discussion

To summarize, cloud drop concentrations in Florida cumulus were observed to vary from 300 cm^{-3} to 2300 cm^{-3}, and this is driven primarily by large variations of CCN concentration in this region. The effects of the boundary layer aerosol on cloud microphysics persist through at least the lowest 1 km of the clouds. An aerosol-CDNC

closure is obtained between predicted and observed CDNC with a bias within the experimental uncertainty of 20%, and variability in model-observation agreement within ~15%, which is comparable to that expected due to experimental sampling limitations. The above closures assume ammonium bisulfate aerosol composition. The CCN closure exhibits variability with a 17% standard deviation which is found to be related to composition, as inferred from the observed hygroscopic growth and the organic carbon to sulfate mass ratio.

We can now ask two questions. 1) Given the 14% model-observation agreement for aerosol-CDNC closure and the 10%-20% agreement for aerosol-CCN closure found by *VanReken et al.* [2003], what constraints do these observations place on assumptions entering the models? 2) What are the most important elements for the complete aerosol-CCN-cloud closure, and are there simplifications that can be used in aerosol activation models for this region?

Question 1: Table 3 illustrates the sensitivity of CCN and CDNC to variations in certain key modeling assumptions. Table 3 values are derived for two specific test cases here, but are consistent with the analyses of *Roberts et al.* [2002], *VanReken et al*. [2003], and *Rissman et al*. [2004]. Two quite different cases are chosen as examples, one from the relatively clean marine case on 7/10, and the other from one of the most polluted cases on 7/18. The baseline case corresponds to ammonium bisulfate aerosol, condensation coefficient of 0.06, surface tension of water, no soluble gases, and updraft velocity of 2 m s^{-1}. The accuracy of the CDNC sensitivity tests is +/- 2% due to the size resolution used in the parcel model. The CDNC sensitivity to varying sulfate type (rows

1 and 2 in Table 3) may have somewhat larger uncertainties (~5%) due to simplifications in the parcel model's treatment of sulfate water activity.

The effect of varying modeling assumptions on the CCN spectrum are comparable to the 17% rms variability in aerosol-CCN closure shown in Section 4 and in *VanReken et al.* [2003]. Thus the CCN data do not rule out moderate variations in the chemical assumptions used. The values in Table 3 should be interpreted keeping in mind that predicted CDNC using ammonium bisulfate is, on average, ~15% lower than the observations, which is still within the estimated experimental uncertainty of 20%. The -15% bias in the baseline model-observation difference is opposite to that expected from the neglect of species less soluble than ammonium bisulfate. For example, if one were to infer from the median value of f(RH) shown in Figure 5 that the insoluble fraction was ~50%, then model observation bias would further decrease by approximately 10%. This would increase model-observation bias beyond the estimated experimental uncertainties. Note that the inference of insoluble fraction from the f(RH) data presented in Section 4 is associated with large uncertainties, and this result should not be over interpreted. Both the CCN and the CDNC closures suggest smaller insoluble fractions. However, it is significant that the sign of this discrepancy contrasts with some previous studies, in which a larger-than-measured insoluble fraction was needed in order to obtain closure (see review in *VanReken et al*. [2003]). Moreover, the sign and magnitude of the model-observation discrepancy supports the lower values of water condensation coefficient (~0.06) that have been used over the previous 50 years, as higher values (~0.3 or greater) would increase the model-observation difference beyond the estimated uncertainties.

Question 2: *Twomey* [1959] derived a simple analytical approximation to obtain droplet concentration from updraft velocity and a two parameter fit to the CCN spectrum, $CCN(S) = CS^k$,

$$CDNC = C^{2/(k+2)}\left[\frac{cw^{3/2}}{kB(k/2,3/2)}\right]^{k/(k+2)} \quad (1)$$

where w is updraft velocity, B is the Beta function, and c is a constant that depends on initial parcel thermodynamic state and aerosol chemical properties. In contrast, the parcel model used in the present study performs a detailed numerical integration of the growth equation, where a 200-bin size distribution is derived from a 4-mode lognormal fit to the data, and droplet growth is derived from complete Köhler theory, as opposed to just the supersaturation spectrum. Given the wide range of conditions encountered during CRYSTAL-FACE, it is interesting to test how much added predictive ability is achieved by using the more detailed calculations. To address this, a series of calculations are made using (1), which are then compared to the more detailed parcel model calculations. First, the parameters C and k are taken from model derived CCN concentrations at 0.2% and 0.85%, and w is taken from the measurements. The small, but finite, 7% standard deviation between the simple Twomey approximation and the detailed calculations is presumably caused by the simplicity of the Twomey expression. Next, the Twomey equation is used as a tool to test which parameters controlled droplet concentration during CRYSTAL FACE. First, the simplest assumption is taken, in which CCN at 0.85% concentration is the only model input from observations; k is fixed at 0.8 (a common assumption) and updraft velocity is fixed at 2 m s^{-1}. The standard deviation between the

detailed model and this simple case is 15%. Thus, CCN at 0.85% together with representative, but fixed, values of updraft velocity and spectral shape match detailed droplet concentration calculations to within 15%. Introducing observed values of k (which range from 0.32 to 0.85) drops the standard deviation only to 13%. Introducing measured updraft velocity with fixed k improves this to 8%, and introducing measured w and k improves the situation marginally to within 7%. When comparing the Twomey model to observations, considering only CCN at 0.85% leaves a variability of 18%, while the full Twomey equation leaves only 13% of the signal unexplained, which is the same as when observations are compared to the detailed model.

In conclusion, this study and that of *VanReken et al.* [2003] have obtained closure among simultaneous measurements of aerosol physical properties, CCN concentrations, cloud drop concentrations, and models that use simple chemistry within the experimental accuracy of ~20%. The degree of closure of 20% in this subtropical region with urban and maritime influences rules out any anomaly of the magnitude reported by some previous studies (see review in *VanReken et al.* [2003]) that were conducted in different regions. Previous studies may have been influenced by differing aerosol compositions among the regions, differing cloud dynamics, and different measurement and analysis techniques. The degree of closure is not sufficiently precise to constrain certain chemical effects on cloud activation that have magnitudes less than 20% (Table 3). This study provides hope that future measurements using similar closure strategies together with improved experimental techniques will afford better accuracy in understanding aerosol-cloud interactions.

Acknowledgments. This work was supported by National Aeronautics and Space Administration grant NAG5-11549 and the Office of Naval Research.

References

Ackerman, A.S., O.B. Toon, J.P. Taylor, D.W. Johnson, P.V. Hobbs, and R.J. Ferek (2000), Effects of aerosols on cloud albedo: Evaluation of Twomey's parameterization of cloud susceptibility using measurements of ship tracks, *J. Atmos. Sci., 57*, 2684-2695.

Albrecht, B.A. (1989), Aerosols, cloud microphysics, and fractional cloudiness, *Science, 245*, 1227-1230.

Baumgardner, D., H. Jonsson, W. Dawson, D. O'Connor, and R. Newton (2001), The cloud, aerosol and precipitation spectrometer: a new instrument for cloud investigations, *Atmos. Res., 59-60,* 251-264.

Bower, K.N., and T.W. Choularton (1988), The effects of entrainment on the growth of droplets in continental cumulus clouds, *Quart. J. Royal Met. Soc., 114*,1411-1434.

Brechtel, F.J., and S.M. Kreidenweis (2000), Predicting particle critical supersaturation from hygroscopic growth measurements in the humidified TDMA. Part I: Theory and sensitivity studies, *J. Atmos. Sci., 57*, 1854-1871.

Burnet, F., and J.-L. Brenguier (2002), Comparison between Standard and Modified Forward Scattering Spectrometer Probes during the Small Cumulus Microphysics Study, *J. Atmos. Oceanic Technol., 19*, 1516-1531.

Chuang, P.Y., D.R. Collins, H. Pawlowska, J.R. Snider, H.H. Jonsson, J.L. Brenguier, R.C. Flagan, and J.H. Seinfeld (2000), CCN measurements during ACE-2 and their relationship to cloud microphysical properties, *Tellus, 52B*, 842-866.

Clarke, A., V. Kapustin, S. Howell, K. Moore, B. Leinert, S. Masonis, T. Anderson, and D. Covert (2003), Sea-salt size distributions from breaking waves: Implications for marine aerosol production and optical extinction measurements during SEAS, *J. Atmos. Oceanic Technol., 20*, 1362-1374.

Draxler, R.R. (1999), Hybrid Single-Particle Lagrangian Integrated Trajectories (HY-SPLIT), Version 4.0: Users Guide. NOAA Technical Memorandum ERL ARL-230, 35 pp., Silver Spring, MD.

Dye, J.E., and D. Baumgardner (1984), Evaluation of the Forward Scattering Spectrometer Probe, *J. Atmos. Oceanic Technol*., *1,* 329-344.

Facchini, M.C., M. Mircea, S. Fuzzi, and R.J. Charlson, Cloud albedo enhancement by surface-active organic solutes in growing droplets (1999), *Nature, 401*, 257-259.

Feingold, G., and P. Chuang (2002), Analysis of the influence of film-forming compounds on droplet growth: Implications for cloud microphysical processes and climate, *J. Atmos. Sci., 59,* 2006-2018.

Fitzgerald, J.W., and P. Spyers-Duran (1973), Changes in cloud nucleus concentration and cloud droplet size distribution associated with pollution from St. Louis, *J. Appl. Meteorol.*, *30*, 511-516.

Gysel M., E. Weingartner, S. Nyeki, D. Paulsen, U. Baltensperger, I. Galambos, and G. Kissn (2004), Hygroscopic properties of water-soluble matter and humic-like organics in atmospheric fine aerosol, *Atmos. Chem. Phys., 4,* 35-50.

Houghton, J.T., Y. Ding, D.J. Griggs, M. Noguer, P.J. van der Linden, X. Dai, K. Maskell, and C.A. Johnson (Eds.) (2001), *Climate Change 2001: The scientific basis. Contribution of Working Group I to the Third Assessment Report of the Intergovernmental Panel on Climate Change*, 881 pp., Cambridge Univ. Press, New York.

Kreidenweis S.M., C.J. Walcek, G. Feingold, W. Gong, M.Z. Jacobson, C.H. Kim, X. Liu, J.E. Penner, A. Nenes, and J.H. Seinfeld (2003), Modification of aerosol mass and size distribution due to aqueous-phase SO_2 oxidation in clouds: Comparisons of several models, *J. Geophys. Res., 108*(D7), 4213, doi:10.1029/2002JD002697.

Laaksonen, A., P. Korhonen, M. Kulmala, and R.J. Charlson (1998), Modification of the Köhler equation to include soluble trace gases and slightly soluble substances, *J. Atmos. Sci., 55*, 853-862.

Lawson, R.P., and A.M. Blyth (1998), A comparison of optical measurements of liquid water content and drop size distribution in adiabatic regions of Florida cumuli, *Atmos. Res., 48*, 671-690.

Lenschow, D. H. (1986), Aircraft measurements in the boundary layer. *Probing the Atmospheric Boundary Layer,* D. H. Lenschow (Ed.), 39–55, Amer. Meteor. Soc., Boston.

Liu, Y.G., and P.H. Daum (2002), Anthropogenic aerosols - Indirect warming effect from dispersion forcing, *Nature, 419,* 580-581.

McFarquhar, G.M., and A.J. Heymsfield (2001), Parameterizations of INDOEX microphysical measurements and calculations of cloud susceptibility: Applications for climate studies, *J. Geophys. Res., 106*, 28675-28698.

Nenes, A., R.J. Charlson, M.C. Facchini, M. Kulmala, A. Laaksonen, and J.H. Seinfeld (2002), Can chemical effects on cloud droplet number rival the first indirect effect? *Geophys. Res. Lett., 29*(17), 1848, doi:10.1029/2002GL015295.

Nenes, A., and J.H. Seinfeld (2003), Parameterization of cloud droplet formation in global climate models, *J. Geophys. Res., 108*(D14), 4415, doi:10.1029/2002JD002911.

Prenni, A.J., P.J. De Mott, and S.M. Kreidenweis (2003), Water uptake of internally mixed particles containing ammonium sulfate and dicarboxylic acids, *Atmos. Env., 37*, 4232-4251.

Pruppacher, H.R., and J.D. Klett (1997), *Microphysics of clouds and precipitation,* 2nd rev., 954 pp., Kluwer Academic Publishers, Boston.

Rissman, T.A., A. Nenes, and J.H. Seinfeld (2004), Chemical amplification (or dampening) of the Twomey effect: Conditions derived from droplet activation theory, *J. Atmos. Sci, 61,* 919-930.

Rivera-Carpio, C.A., C.E. Corrigan, T. Novakov, J.E. Penner, C.F. Rogers, and J.C. Chow, Derivation of contributions of sulfate and carbonaceous aerosols to cloud condensation nuclei from mass size distributions (1996)*, J. Geophys. Res., 101,* 19,483-19,493.

Roberts, G. C., P. Artaxo, J. Zhou, E. Swietlicki, and M. O. Andreae (2002), Sensitivity of CCN spectra on chemical and physical properties of aerosol: A case study from the Amazon Basin, *J. Geophys. Res., 107*, 8070, doi:10.1029/2001JD00583.

Rosenfeld, D., and I.M. Lensky (1998), Satellite-based insights into precipitation formation processes in continental and maritime convective clouds, *Bull. Am. Met. Soc., 79*, 2457-2476.

Segal Y., M. Pinsky, A. Khain, and C. Erlick (2003), Thermodynamic factors influencing bimodal spectrum formation in cumulus clouds, *Atmos. Res., 66,* 43-64.

Shaw, R.A. (2003), Particle-turbulence interactions in atmospheric clouds, *Ann. Rev. Fluid Mech., 35*, 183-227.

Shaw, R.A., and D. Lamb (1999), Experimental determination of the thermal accommodation and condensationcoefficients of water, *J. Chem. Phys., 111,* 10659-10663.

Shulman, M.L., M.C. Jacobson, R.J. Charlson, R.E. Synovec, and T.E. Young (1996), Dissolution behaviour and surface tension effects of organic compounds in nucleating cloud droplets, *Geophys. Res. Lett., 23*, 277-280.

Snider, J.R., and J.-L. Brenguier (2000), Cloud condensation nuclei and cloud droplet measurements during ACE-2, *Tellus, 52B*, 828-842.

Snider, J.R., S. Guibert, J.-L. Brenguier, and J.P. Putaud (2003), Aerosol activation in marine stratocumulus clouds: 2. Kohler and parcel theory closure studies, *J. Geophys. Res., 108*(D15), 8629, doi:10.1029/2002JD002692.

Twomey, S. (1959), The nuclei of natural cloud formation part II: The supersaturation in natural clouds and the variation of cloud droplet concentration, *Geofis. Pura. Appl., 43,* 243-249.

Twomey, S. (1977), The influence of pollution on the shortwave albedo of clouds, *J. Atmos. Sci., 34,* 1149-1152.

Twomey, S., and J. Warner (1967), Comparison of measurements of cloud droplets and cloud nuclei, *J. Atmos. Sci., 24*, 702-703.

VanReken, T.M., T.A. Rissman, G.C. Roberts, V. Varutbangkul, H.H. Jonsson, R.C. Flagan, and J.H. Seinfeld (2003), Toward aerosol/cloud condensation nuclei (CCN) closure during CRYSTAL-FACE, *J. Geophys. Res., 108*(D20), 4633, doi:10.1029/2003JD003582.

Table 1: Aerosol, cloud and meteorological instrumentation for ONR's CIRPAS Twin Otter aircraft during CRYSTAL-FACE.

Measurement	Instrument	Measurement Parameters	Measurement Principle
Aerosol Concentration	Condensation Particle Counters (3)	Geometric Diameter > {3 nm, 7 nm, 13 nm}	Varying Supersaturations of Butanol
Aerosol Size distribution	Dual Autostatic Classifier Detector System (DACADS)	Geometric Diameter: 15 nm – 800 nm	Electrostatic Classification; Dry and Ambient Humidity
	Aerosol Spectrometer Probe (PCASP)	Geometric Diameter: 100 nm – 2500 nm	Optical Scattering
	Aerodynamic Paricle Sizer (APS)	Aerodynamic Diameter: 500 nm – 10 000 nm	Aerodynamic Classification
Cloud and Aerosol Size distribution	Forward Scattering Spectrometer Probe (FSSP)	Geometric Diameter: 3 μm – 47 μm	Optical Forward Scattering
	Cloud and Aerosol Particle Spectrometer (CAPS)	Geometric Diameter: 0.5 μm – 1600 μm	Optical Forward Scattering and 2D Imaging
CCN Concentration	Caltech CCN Counter	$S_C < 0.85\%$	Continuous flow; Increasing temperature
	Scripps CCN Counter	$S_C < 0.2\%$	
Aerosol Composition	Aerodyne Aerosol Mass Spectrometer (AMS)	Mass Concentration: SO_4^{2-}, NH_4^+, NO_3^-, OC 100 nm – 600 nm	Flash ionization; Quadraplole Mass spectromemeter
Updraft velocity and wind speed	5-hole turbulence Probe, CMIGITS internal navigation system and Novatel GPS	Wind velocity; aircraft position and attitude	Wind velocity = Aircraft ground velocity (CMIGITS INS/GPS) - Aircraft air velocity (turbulence and pitot-static probes)

Table 2: Summary of cloud observations.

Flight # - Cloud #	Date (mo/dy)	# Passes (Below/In)	CCN 0.85% (cm^{-3})	σ CCN (cm^{-3})	N_A (cm^{-3}) (35-800 nm)	OC/SO_4 mass ratio (100-600 nm)	w (ms^{-1})	N_D (cm^{-3}) predicted	N_D (cm^{-3}) Observed	
									Method 1	Method 2
H4-1	6/27	2/4	764	53	811	0.16	1.4	626	769	820
H4-2	6/27	2/3	1062	97	1049	0.15	1.0	699	959	1177
H4-3	6/27	2/11	515	17	510	0.13	0.9	382	413	409
C4	7/7	3/6	860	129	1025	0.4	2.2	830	1042	1427
C6-1	7/10	1/6	343	20	294	0.3	0.9	220	216	275
C6-2	7/10	2/11	407	156	309	0.3	1.8	279	280	272
C6-3	7/10	1/7	569	103	612	0.3	1.0	400	434	392
C8-1	7/13	1/6	N/A	N/A	1167	1.3	1.5	847	1078	1277
C8-2	7/13	1/5	N/A	N/A	1034	1.5	1.9	938	936	935
C10-1	7/18	1/5	2785	124	3394	2.4	1.5	2239	2285	2279
C10-2	7/18	1/5	2783	111	3350	2.5	1.2	1893	1995	2167
C11-1	7/18	1/7	1746	40	1879	1.9	2.8	1666	1717	1959
C11-2	7/18	2/5	2520	210	3007	2.5	2.4	2358	2526	2667
C12-1	7/19	1/12	561	65	478	N/A	2.4	469	523	575
C12-2	7/19	2/8	450	215	410	N/A	2.2	397	633	641
C16-1	7/25	1/5	316	18	348	0.6	1.1	273	360	390
C16-2	7/25	1/3	316	18	348	0.5	1.6	312	330	426
C17-1	7/26	2/6	454	43	455	0.4	1.7	384	423	419
C17-2	7/26	1/7	305	30	373	0.3	1.6	306	493	363
C17-3	7/26	1/9	N/A	N/A	681	0.3	2.4	614	N/A	642
C20*	7/29	1/1	967	387	1797	1.0	2.8	1225	1167	1167

* This was a brief pass into the base of a larger convective system.

Table 3: Effects of changing model assumptions on predicted CCN and CDNC (See text).

	CCN 0.2%		CCN 0.85%		CDNC	
	C10.1	C6.1	C10.1	C6.1	C10.1	C6.1
$(NH_4)_2SO_4$	-1.5%	-1.2%	-0.2%	-0.9%	+4%	+5%
H_2SO_4*	-15%	-13%	-3%	-10%	-13%	-24%
50% insoluble (externally mixed)	-50%	-50%	-50%	-50%	-28%	-41%
50% insoluble (internally mixed)	-23%	-21%	-5%	-19%	-5%	-15%
20% surface tension reduction	+18%	+19%	+5%	+15%	+8%	+11%
50% insoluble (internal) and 20% surface tension reduction	-2%	-1%	0%	-1%	+4%	+0%
Updraft + 0.35 m s^{-1}	N/D	N/D	N/D	N/D	+8%	+5%
Condensation coeff. = 0.03	N/D	N/D	N/D	N/D	+11%	+10%
Condensation coeff. = 0.3	N/D	N/D	N/D	N/D	-9%	-10%

* The sulfuric acid calculations include 35% H_2O by weight to the dry size distribution due to the fact that "dry" aerosol size distribution is measured at 15%-20% RH. The other sulfate species are assumed to be crystallized below 20% RH
N/D = Not a model dependent parameter.

Figure 1: Map of the CRYSTAL-FACE region in S. Florida. Each symbol denotes the location of a cloud characterized by the Twin Otter.

Figure 2: Aerosol-CDNC closure. Predicted vs. observed droplet concentration. Observed values use Method 1 screening (see text) for adiabaticity. The short-dashed line represents an unweighted least-squares linear fit to the data in log-log units. The long-dashed line represents a fit to the data when Method 2 screening is used. The solid line represents perfect model-observation agreement. The term "cloud base" reiterates that observations used in this plot were generally taken in adiabatic regions within 100 m of cloud base.

Figure 3: CCN-forced variations in CDNC and influence on the vertical profile of effective radius. The stated CCN and CDNC values for each cloud were obtained below-cloud and within 100 m of cloud base, respectively. Solid lines are adiabatic predictions using observed sub-cloud thermodynamic properties and observed CDNC within 50 m of cloud base.

Figure 4. Illustration of Methods 1 and 2 (see text) for determining hygroscopic growth factor from the DACADS data. A) Dry and humid (55% RH) size distribution for measurements below 800 m altitude in the vicinity of clouds H4.1 and H4.2. The lognormal fitting is shown as dashed lines. The fitted parameters and Method 2 f(RH=55%) values are shown for each mode. B) Cumulative size distributions from (A)

above, plotted as a function of dry diameter with the Method 1 hygroscopic growth factor. Truncation in the size distribution limits accuracy beyond 300 nm.

Figure 5. A) Effective cutoff diameter for S_C=0.85% plotted vs. f(RH) for the Aitken mode using Method 2. Diamonds are overland flights, asterisks are marine flights, and pluses are data from the marine flight C6 (discussed in text). Model simulations for $(NH_4)_2SO_4$ mixed internally with the indicated volume fraction of insoluble material are shown as connected squares. The f(RH) in the model calculations curve corresponds to 63% RH, and the range bars represent values from 59% to 69% (median values for ocean and land, respectively). B) f(RH) plotted vs. humid DMA RH for the same points as in Figure 5A. The curves corresponds to uncrystallized $(NH_4)_2SO_4$. The solid curve represents pure sulfate, the dashed curve represents sulfate internally mixed with an equal volume of insoluble material. (50% OC by volume would correspond to about 35% OC by mass).

Figure 6. Percent difference between observed CCN(0.85%) and $N(d > 32$ nm) obtained from the DMA plotted as a function of f(RH) of the Aitken mode. Symbols are same as those in Fig. 5.

Figure 7. Relationship between D_C(0.85%) and AMS measured organic carbon to sulfate mass ratio.

Figure 8: A) Relationship between Aitken mode *f*(RH) and AMS measured organic carbon to sulfate mass ratio for OC:SO_4^{2-} ratios below 0.5. B) Same as A, but for accumulation mode *f*(RH).

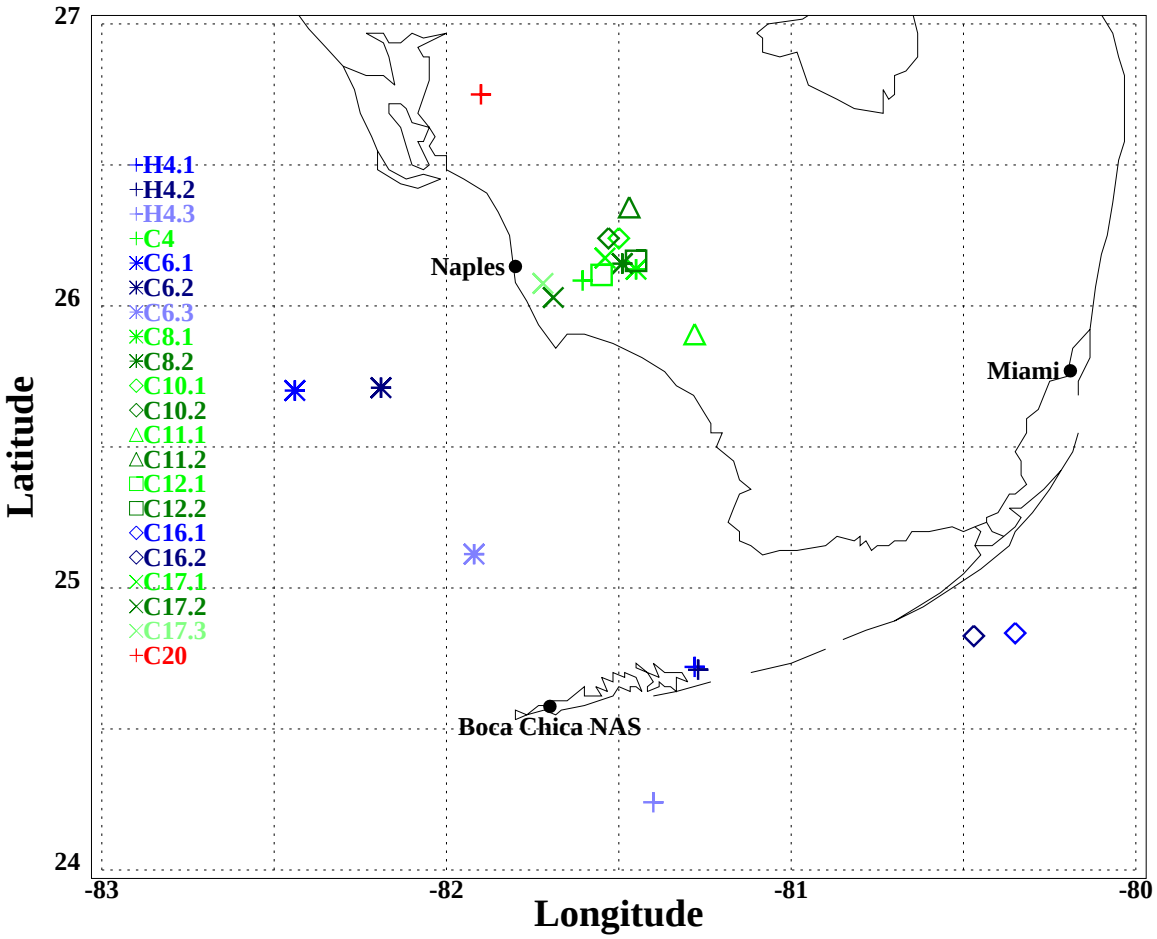
27
26
25
24
-83
-82
-81
-80
Latitude
Longitude
Naples
Miami
Boca Chica NAS
+H4.1
+H4.2
+H4.3
+C4
✳C6.1
✳C6.2
✳C6.3
✳C8.1
✳C8.2
◇C10.1
◇C10.2
△C11.1
△C11.2
□C12.1
□C12.2
◇C16.1
◇C16.2
×C17.1
×C17.2
×C17.3
+C20

Figure 1.

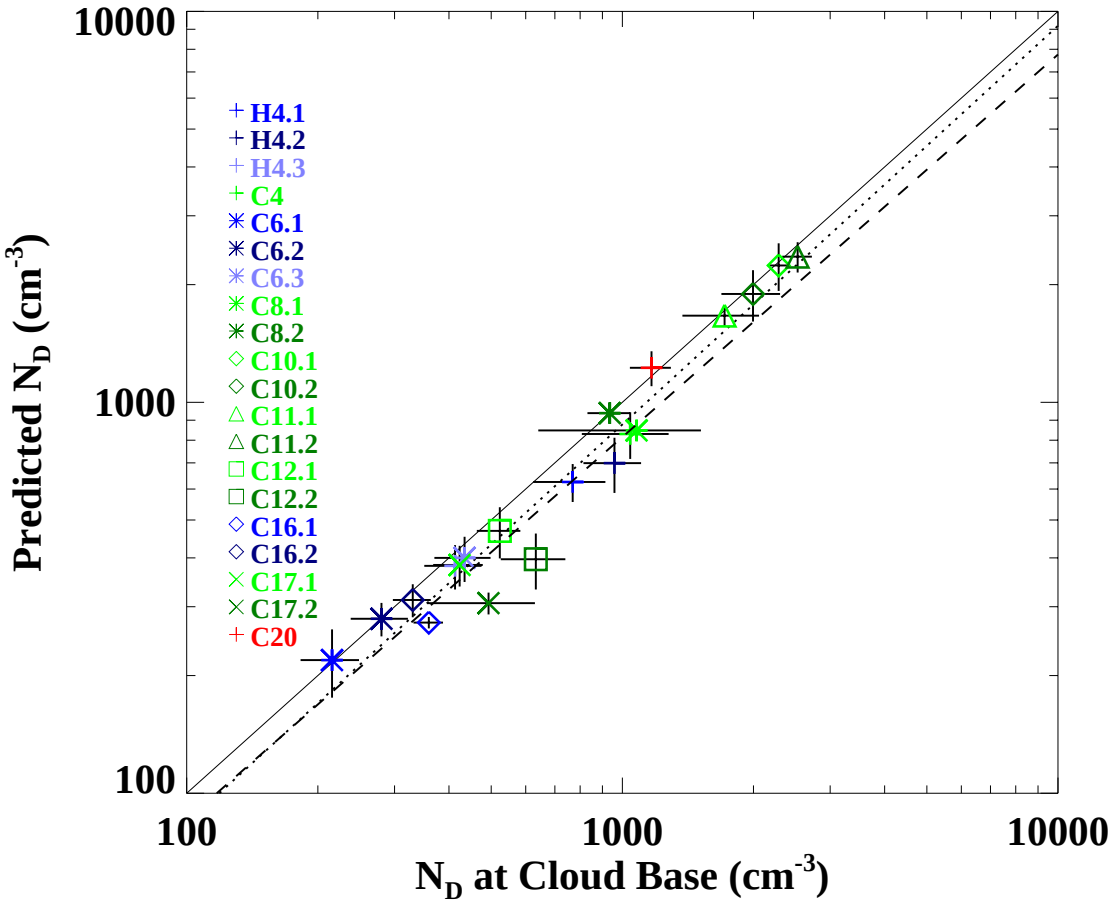
10000
1000
100
100
1000
10000
Predicted N_D (cm^{-3})
N_D at Cloud Base (cm^{-3})
H4.1
H4.2
H4.3
C4
C6.1
C6.2
C6.3
C8.1
C8.2
C10.1
C10.2
C11.1
C11.2
C12.1
C12.2
C16.1
C16.2
C17.1
C17.2
C20

Figure 2.

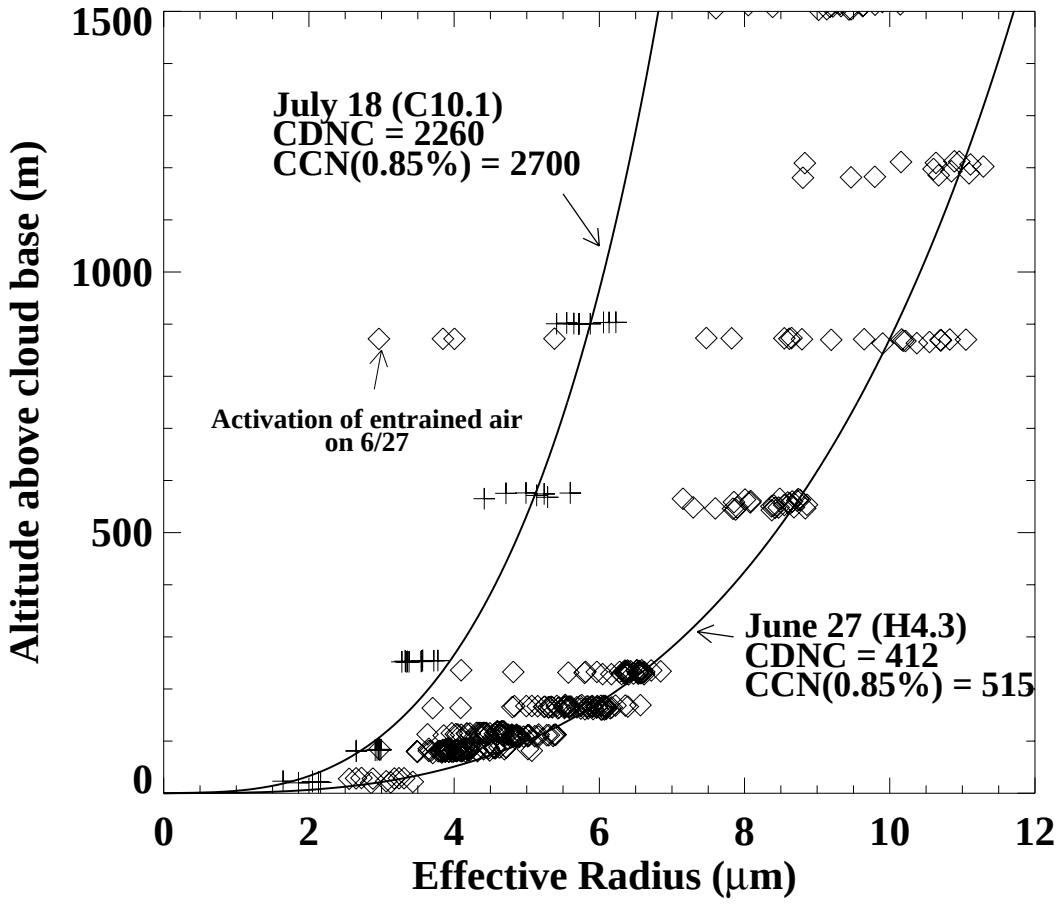
1500
1000
500
0
Altitude above cloud base (m)
July 18 (C10.1)
CDNC = 2260
CCN(0.85%) = 2700
Activation of entrained air
on 6/27
June 27 (H4.3)
CDNC = 412
CCN(0.85%) = 515
0
2
4
6
8
10
12
Effective Radius (μm)

Figure 3.

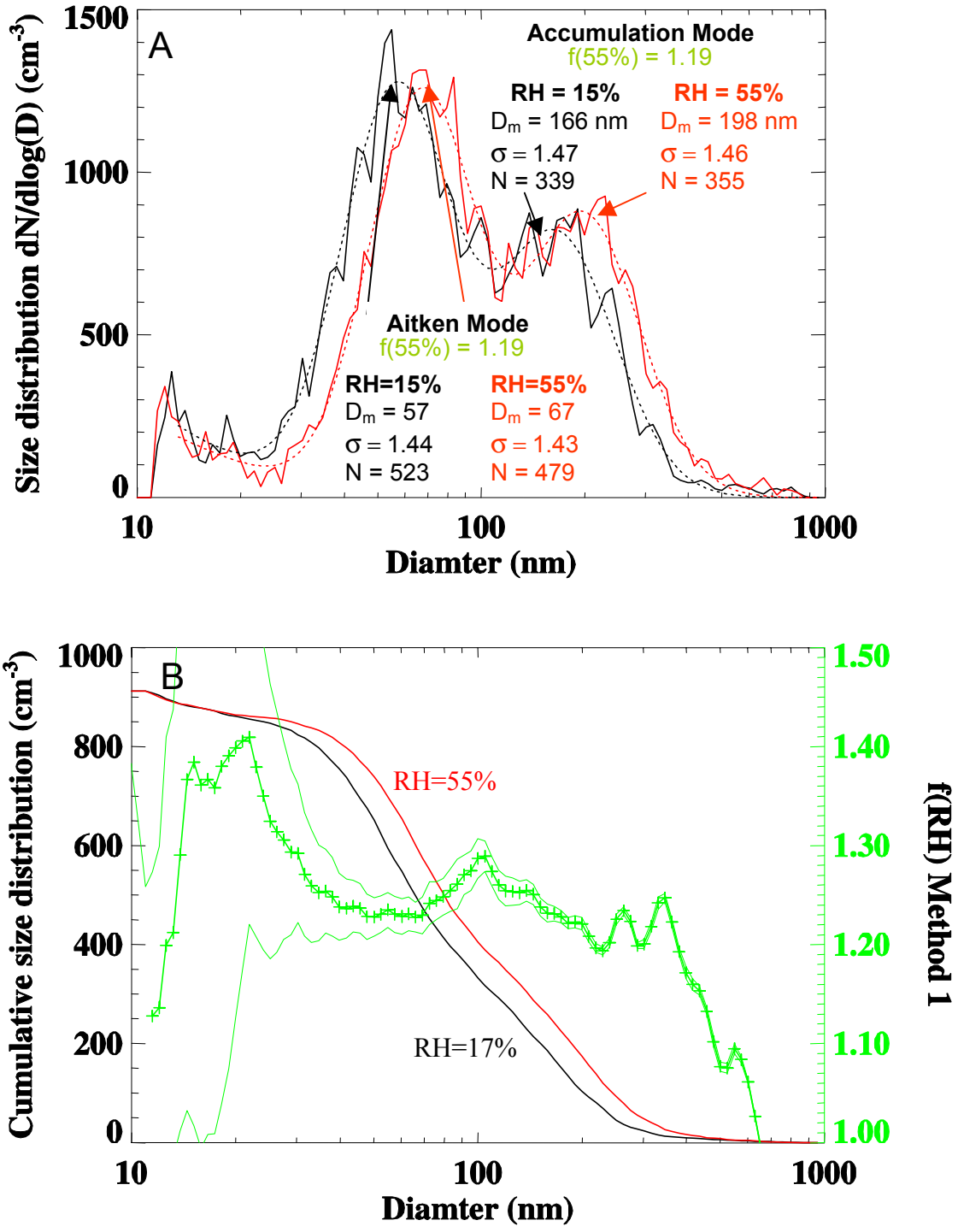
A
Accumulation Mode
f(55%) = 1.19
RH = 15%
Dm = 166 nm
σ = 1.47
N = 339
RH = 55%
Dm = 198 nm
σ = 1.46
N = 355
Aitken Mode
f(55%) = 1.19
RH=15%
Dm = 57
σ = 1.44
N = 523
RH=55%
Dm = 67
σ = 1.43
N = 479
Size distribution dN/dlog(D) (cm-3)
Diamter (nm)
B
RH=55%
RH=17%
Cumulative size distribution (cm-3)
f(RH) Method 1
Diamter (nm)

Figures 4A,B.

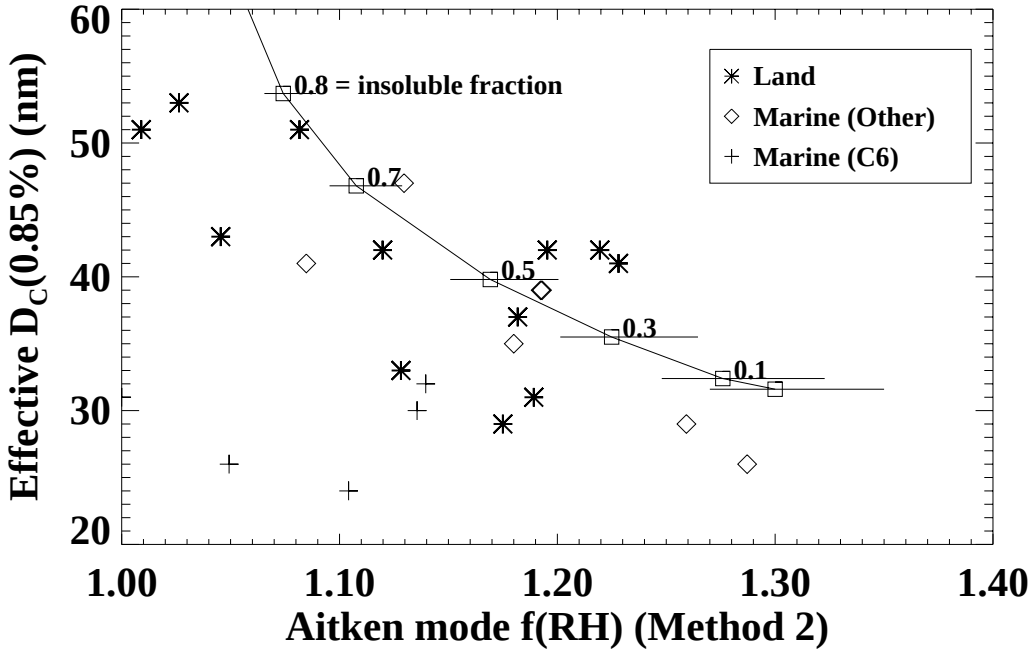
Effective D_C(0.85%) (nm)
60
50
40
30
20
1.00
1.10
1.20
1.30
1.40
Aitken mode f(RH) (Method 2)
0.8 = insoluble fraction
0.7
0.5
0.3
0.1
Land
Marine (Other)
Marine (C6)

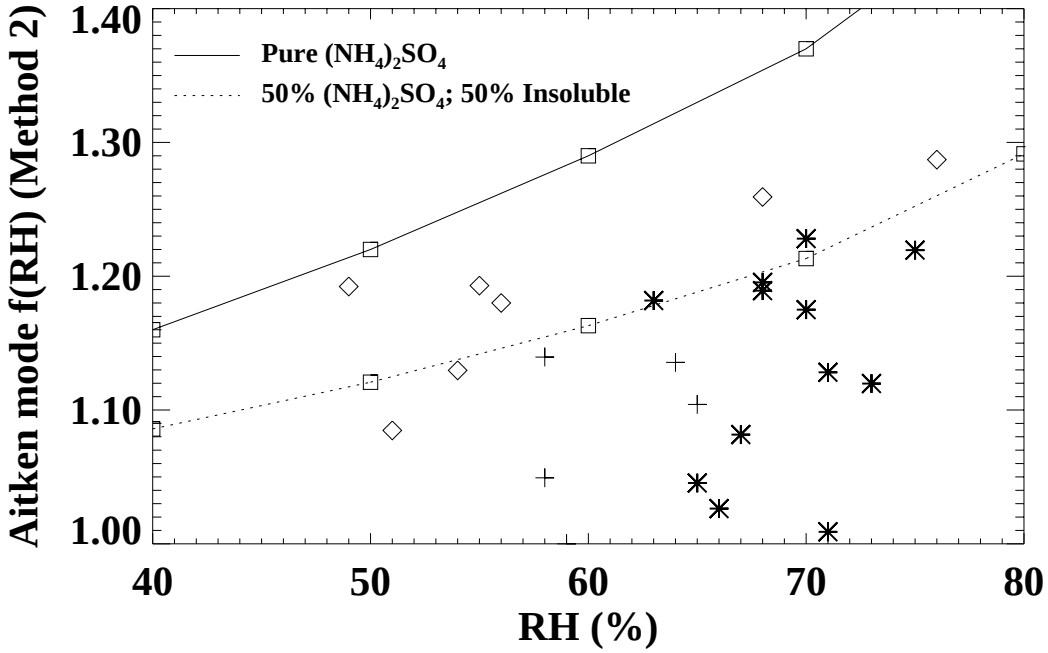
Aitken mode f(RH) (Method 2)
1.40
1.30
1.20
1.10
1.00
40
50
60
70
80
RH (%)
Pure $(NH_4)_2SO_4$
50% $(NH_4)_2SO_4$; 50% Insoluble

Figures 5A,B.

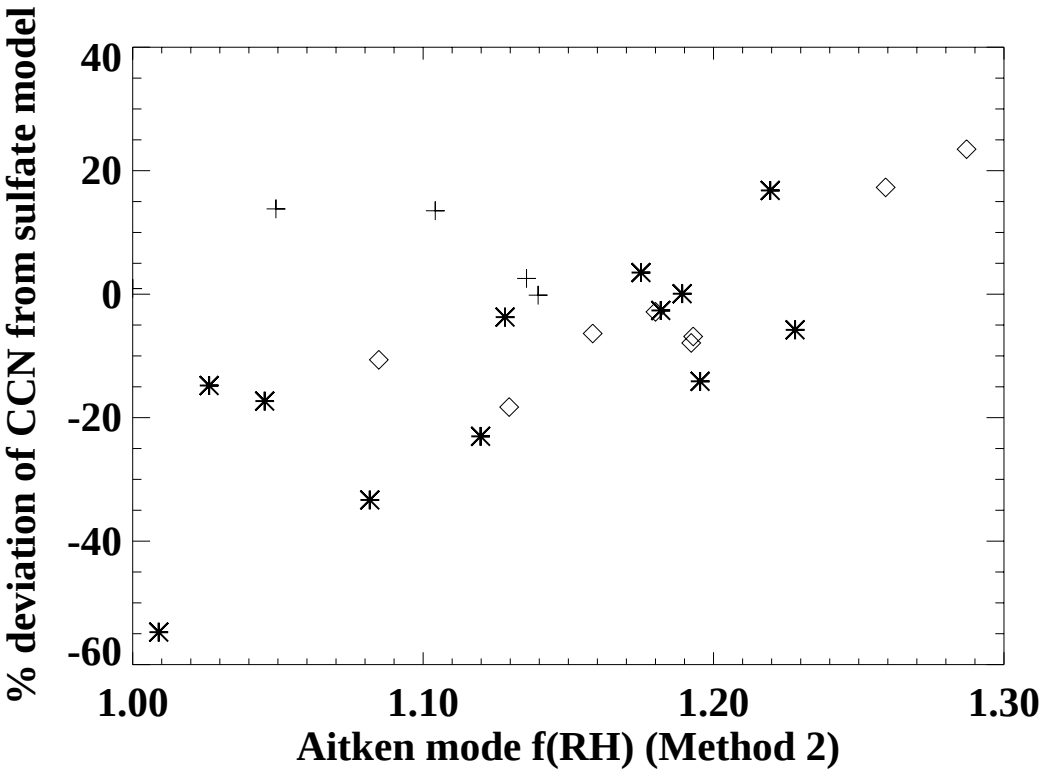
% deviation of CCN from sulfate model
40
20
0
-20
-40
-60
1.00
1.10
1.20
1.30
Aitken mode f(RH) (Method 2)

Figure 6.

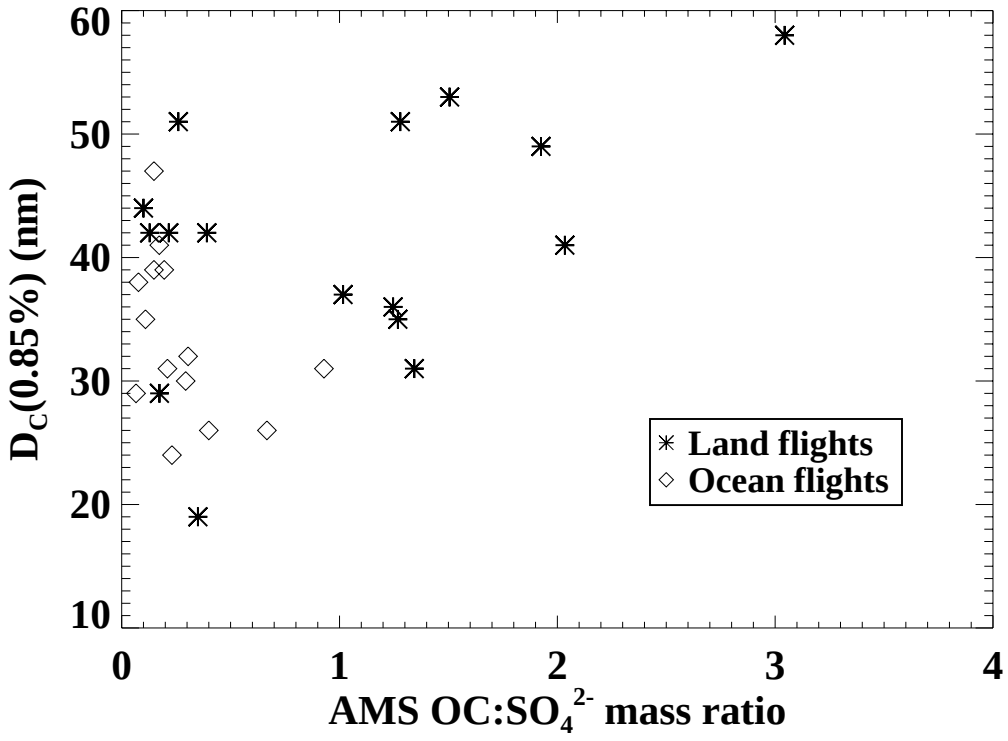
60
50
40
30
20
10
0
1
2
3
4
D_C(0.85%) (nm)
AMS OC:SO_4^{2-} mass ratio
Land flights
Ocean flights

Figure 7.

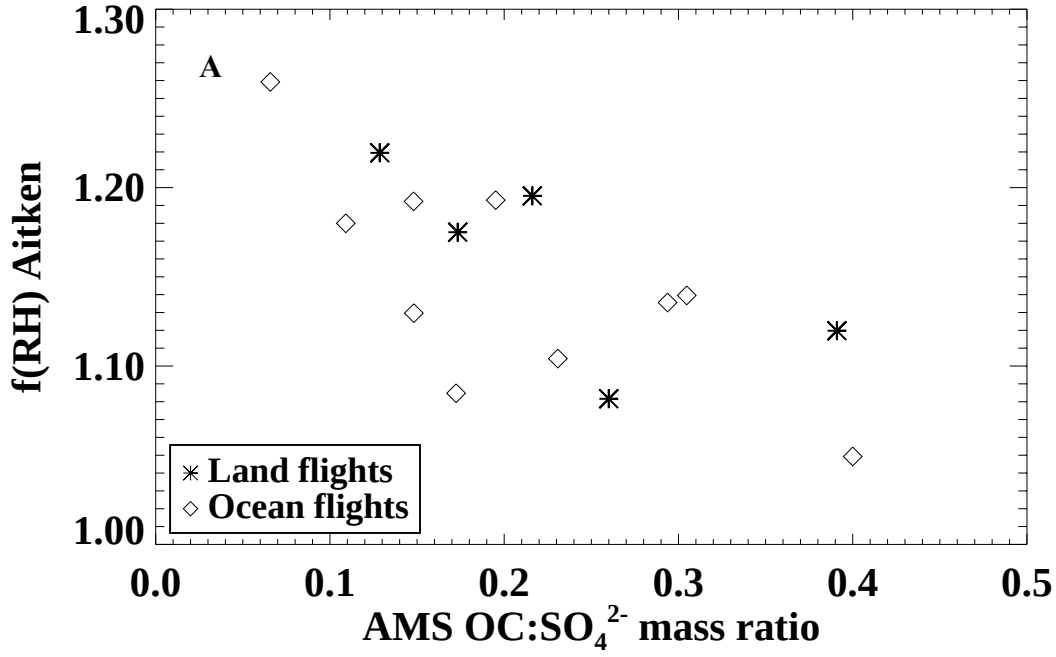
A
f(RH) Aitken
1.30
1.20
1.10
1.00
0.0
0.1
0.2
0.3
0.4
0.5
Land flights
Ocean flights
AMS OC:SO4 2- mass ratio

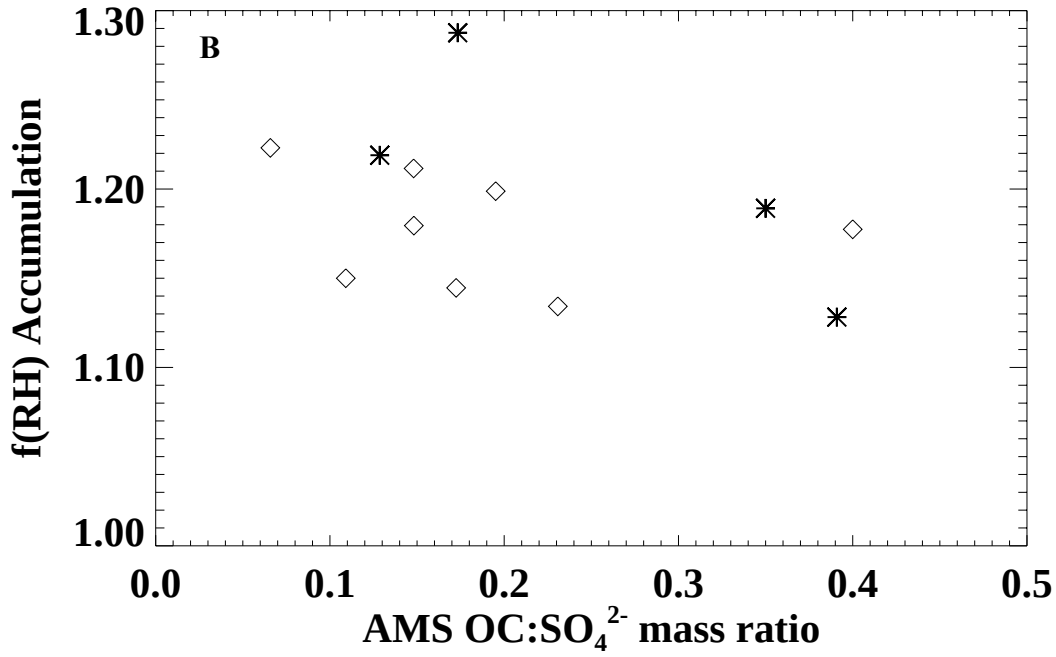
B
f(RH) Accumulation
1.30
1.20
1.10
1.00
0.0
0.1
0.2
0.3
0.4
0.5
AMS OC:SO4 2- mass ratio

Figures 8A,B.